

Article

Long-Lasting Boiling-Wells: Geochemical Windows into the Tectonic Activity of the Maodong Fault (China)

Lin Liu ^{1,2,3}, Yuehua Jiang ^{2,3,*}, Xun Zhou ^{2,3}, Yun Li ^{2,3}, Quanping Zhou ^{2,3}, Jingwen Su ^{2,3}, Junyuan Jia ^{2,3}, Guoqiang Yang ^{2,3} and Yang Jin ^{1,2,3}

¹ Chinese Academy of Geological Sciences, Beijing 100037, China; liulin@mail.cgs.gov.cn (L.L.); sdkjdxjy@163.com (Y.J.)

² Nanjing Center, China Geological Survey, Nanjing 210016, China; weapon341@163.com (X.Z.); liyun@mail.cgs.gov.cn (Y.L.); zhouquanping@mail.cgs.gov.cn (Q.Z.); sujw@mail.cgs.gov.cn (J.S.); jiajunyuan828@163.com (J.J.); yangguoqiang@mail.cgs.gov.cn (G.Y.)

³ Key Laboratory of Watershed Eco-Geological Processes, Ministry of Natural Resources, Nanjing 210016, China

* Correspondence: jyuehua@mail.cgs.gov.cn

Abstract: The Maodong Fault (China) was mainly active during the Late Pleistocene. However, in the past century, numerous destructive earthquakes have occurred along the fault zone, indicating its continuing activity. Therefore, refined monitoring of the tectonic activity along the fault is required. Boiling-Wells located in the Maodong Fault Zone were selected for this purpose. The parameters, including the rare earth elements (REE) and gas components, such as CO₂, Rn, and Total Volatile Organic Compounds (TVOC), in the wells were analyzed. By combining field observations with the analytical data, we constrained the relationships between the anomalies of the hydrochemical composition and the gas composition in the Boiling-Wells and the Maodong Fault: (1) CO₂ and TVOC in the Boiling-Wells originated from Cenozoic magmatism and associated intrusive rocks. High concentrations of Rn are closely linked to tectonic activities of the Maodong Fault. CO₂, TVOC, and Rn are all transported to the Boiling-Wells along the Maodong Fault, with CO₂ acting as a carrier gas for Rn. (2) REE in the Boiling-Wells was mainly sourced from CO₂ fluids that originated from deep-seated Cenozoic magmas and intrusive rocks. The concentrations of the REE and their distribution patterns were controlled by the input of CO₂ fluids and by epigenetic processes. (3) The abnormally high contents of Ca²⁺, HCO₃⁻, Pb²⁺, and Al³⁺ in the Boiling-Wells are attributed to the migration of externally-derived (deep) CO₂ fluids through the Maodong Fault. (4) The anomalies of the gaseous (Rn, CO₂, and TVOC) and hydrochemical components (Ca²⁺, HCO₃⁻, Pb²⁺, Al³⁺, ΣREE, and REE patterns) in the Boiling-Wells are closely related to the tectonic activity of the Maodong Fault. Therefore, the long-lasting Boiling-Wells provide an excellent geochemical window into the evolution of the Maodong Fault. Our study documents that the contents and variations of specific hydrochemical and gaseous components of Boiling-Wells are well-suited geochemical tracers to identify and characterize the tectonic activity of the Maodong Fault. This method is also applicable for the monitoring of tectonic activities of major faults zones with comparable preconditions worldwide.

Keywords: long-lasting Boiling-Wells; Maodong Fault; CO₂; rare earth elements (REE); geochemical anomaly



Citation: Liu, L.; Jiang, Y.; Zhou, X.; Li, Y.; Zhou, Q.; Su, J.; Jia, J.; Yang, G.; Jin, Y. Long-Lasting Boiling-Wells: Geochemical Windows into the Tectonic Activity of the Maodong Fault (China). *Water* **2022**, *14*, 427. <https://doi.org/10.3390/w14030427>

Academic Editors: Fernando António Leal Pacheco and Aldo Fiori

Received: 12 December 2021

Accepted: 28 January 2022

Published: 29 January 2022

Publisher's Note: MDPI stays neutral with regard to jurisdictional claims in published maps and institutional affiliations.



Copyright: © 2022 by the authors. Licensee MDPI, Basel, Switzerland. This article is an open access article distributed under the terms and conditions of the Creative Commons Attribution (CC BY) license (<https://creativecommons.org/licenses/by/4.0/>).

1. Introduction

Seismic activities along faults or fractures may disturb the original equilibrium state of the water–rock interaction in the crust, resulting in abnormal changes in the chemical composition of gas and water in the groundwater [1–6]. Long-term observations have shown that the composition of groundwater near the Earth's surface and the gas composition in the soil sensitively record the stress and strain state of the Earth's crust [7,8]. Fault zones are important locations in the continental crust for the release of gases [9–12]. Previous studies have shown that the concentrations of CO₂, Rn, and other gases in the

water and soil of the fault zones are often higher than those in the adjoining areas [9–12]. For instance, the contents of Cl^- and SO_4^{2-} in nearby groundwater fluctuated and rapidly increased eight months before the onset of the Kobe earthquake (M7.2) in 1995 [3]. Before the Jingtai Earthquake (M6.2) in 1990, the contents of HCO_3^- , CO_3^{2-} , and Cl^- in hot springs such as Zhongwei and Shaokou (China) increased by 40% abnormally [13]. Perrier et al. [9] observed CO_2 bubbles that emerged from the deep crust in the Syabru-Bensi hot spring (Nepal), located on the Main Central Thrust zone of Nepal. High contents (16,000–41,000 Bq/m^3) of Rn were observed in the CO_2 bubbles collected in the water of Syabru-Bensi hot spring (Nepal), which were considered to result from degassing in the Himalayas. Meng et al. [14] recognized distinct corresponding relations between the concentrations of Rn and Hg and tectonic activities in the Haiyuan fault zone (China) by analyzing the gas content in the soil. The examples demonstrate that abnormal concentrations of specific gas components in groundwater and soil can be used as indicators for fault activity and as indexes for changes of stress in the crust.

The Liyang M5.5 earthquake in 1974 and the Liyang M6.0 earthquake in 1979 occurred along the Maodong Fault Zone (Figure 1). In addition, earthquakes with a lower magnitude were very frequently recorded along the Maodong Fault Zone and adjoining areas (Figure 1), documenting that the potential of intermediate to strong earthquakes still persists [15–19]. The Maodong Fault Zone runs through highly populated areas in China with large and economically important cities such as Xuancheng, Nanjing, Changzhou, Zhenjiang, Danyang, and Yangzhou (Figure 1). For the safety of the population and the maintenance of the economy, therefore, it is necessary to precisely monitor the activity of the Maodong Fault Zone.

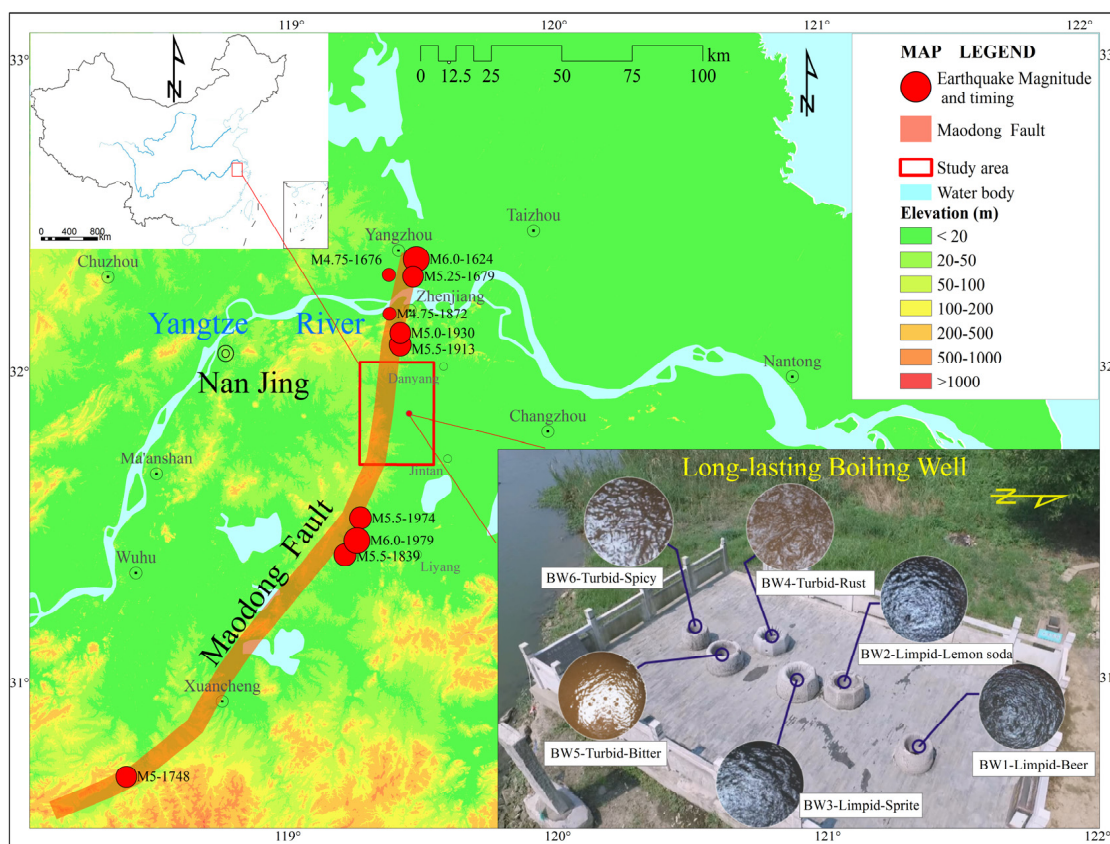


Figure 1. Distribution of destructive earthquakes at the Maodong Fault and the location of the six Long-lasting Boiling-Wells in the Jizi temple (Jiuli village).

Six ancient wells with a history of almost 2000 years occur in the Jizi temple of the Jiuli village (Yanling Town, Danyang City, Jiangsu Province, China (inset in Figure 1)). Due

to abnormally high concentrations of CO₂, Rn, and other constituents degassing from the water [20], the water in the wells appears to boil constantly. Therefore, the six wells are called Boiling-Wells. The depths of Boiling-Wells are 3 to 4 m, and the water temperature is about 19 °C in summer. The six Boiling-Wells are concentrated in a nearly north–south direction following the strike of the fault (inset in Figure 1). The distance between the individual wells is 0.5 m to 10 m (Figure 1).

Due to the variable “boiling” conditions, the taste and color of the well water vary (Figure 1). The water of the three wells in the north is limpid and tastes like beer, lemon, and sprite, whereas that of the three wells in the south is turbid to cloudy and tastes like rust, bitter, and spice. Based on geophysical studies, Jiang et al. [20] detected secondary faults in the Maodong Fault Zone as well as Cenozoic intrusions below the Boiling-Wells. They concluded that the boiling phenomenon is induced by gas that was dissolved in water, rises up along the Maodong Fault, and later degasses in the wells. The gases were dominated by CO₂ and mixed with minor amounts of Rn and total volatile organic compounds (TVOC). In addition, chemical components such as Ca²⁺, HCO₃[−], and rare earth elements (REE) were significantly enriched in the Boiling-wells water compared to water from surrounding shallow wells [20]. However, the origin of the exceptional composition of the boiling-well water (particularly the striking REE enrichment) and its link to the Maodong Fault were uncertain.

We studied the genesis of the geochemical anomalies, including the gas and hydrochemical components, and the REE contents, as well as their distribution pattern in the Boiling-Wells, to elucidate their relationship with the tectonic activity of the Maodong Fault by sampling and analyzing water from the Boiling-Well, surrounding shallow wells, and a nearby lake. The anions, cations, metals, REE, and gas components in water samples were analyzed, and the previously published data of natural shallow groundwater in other plain basins were also collected.

2. Materials and Methods

2.1. Study Area

The study area is located in the Maodong Fault Zone at the eastern margin of the Maoshan Mountain in Danyang City (Jiangsu Province, China; Figure 1). Quaternary sediments cover the Maodong Fault in the study area. The climate of the area is subtropical humid, with an annual average precipitation of 1032.6 mm and evaporation of 1517.7 mm. The shallow groundwater mainly occurs in Quaternary loose sediments that are composed of brownish-yellow silty clay and silty sand [21]. The groundwater is mainly supplied by atmospheric precipitation, and evaporation is the main discharge mode [21].

The Maodong Fault (Figure 1) shows an overall NNE-strike with a dip angle of 35 to 85° and an overall dip toward the southeast [16,19,22]. The fault comprises a series of sub-parallel normal faults that are staggered in steps. The Maodong Fault was mainly active in the Late Pleistocene, but several destructive earthquakes in the past century occurred along the fault zone (Figure 1), indicating that the fault is still active and that the monitoring of the tectonic activity of the fault needs to be strengthened [16].

2.2. Water Sampling

In addition to water samples of the six Boiling-Wells and of a nearby lake that exhibits a comparable boiling phenomenon, we collected samples from shallow groundwater within an area of 10 to 15 km around the Boiling-Wells as references. The distribution of sample locations was shown in Figure 2. All samples represent shallow groundwater that was hosted by loosely accumulated Quaternary silty clay. A total of 40 water samples were collected, including six samples from Boiling-Wells, one sample of the boiling lake, and 33 groundwater samples from less than 10 m depths. For conventional hydrochemical analysis, the sample volume used for the anion test was 1.5 L, which was stored airtight. The volume used for the cation test was 0.5 L, acidified with 5 ml nitric acid to pH < 2 and stored airtight. The volume of water samples used for REE element analysis was 0.5 L, which was packed

in a polyethylene bottle that had been cleaned with acid. Subsequently, the polyethylene bottle was sealed with a sealing film and sent to the laboratory for analysis.

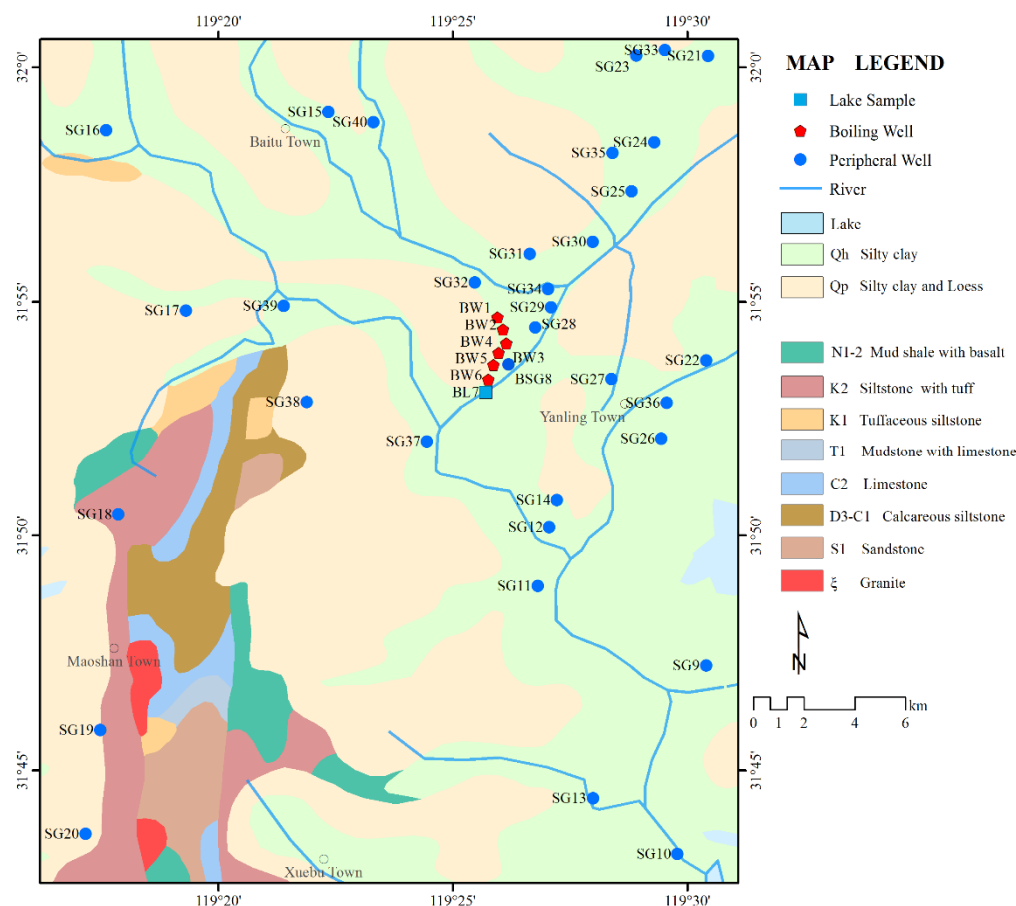


Figure 2. Geological sketch of the study area with the sample locations.

2.3. Analytical Methods

All the samples were measured at the Supervision and Testing Center of East China Mineral Resources (Nanjing, China). The contents of Cl^- , SO_4^{2-} , NO_3^- , and F^- were determined by ion chromatography (Dionex-2500 ion chromatograph, ThermoFisher, Waltham, MA, USA). The detection limit of SO_4^{2-} was 0.08 mg/L, and the detection limit of Cl^- , NO_3^- , and F^- was 0.02 mg/L. The contents of K^+ , Na^+ , Ca^{2+} , Mg^{2+} , Fe^{2+} , and H_2SiO_3 were analyzed by an inductively coupled plasma spectrometer (ICAP 6300Duo, ThermoFisher, Waltham, MA, USA). The detection limits of K^+ , Na^+ , Mg^{2+} , Ca^{2+} , Fe^{2+} , and H_2SiO_3 were 0.02 mg/L, 0.005 mg/L, 0.013 mg/L, 0.011 mg/L, 0.04 mg/L, and 0.02 mg/L, respectively. The contents of Al^{3+} , Mn^{2+} , Pb^{2+} , Zn^{2+} , and I^- were determined by inductively coupled plasma mass spectrometry (ICP-MS (iCAP-Q), ThermoFisher, Waltham, MA, USA). The detection limits of Al^{3+} , Mn^{2+} , Pb^{2+} , Zn^{2+} , and I^- were 5 $\mu\text{g/L}$, 0.1 $\mu\text{g/L}$, 0.5 $\mu\text{g/L}$, 1 $\mu\text{g/L}$, and 10 $\mu\text{g/L}$, respectively. The contents of dissolved free CO_2 HCO_3^- were measured by titration with a detection limit of 3 mg/L. The contents of As and Se were analyzed by atomic fluorescence spectrometry (AFS-9600, Haiguang Instrument, Beijing, China) with detection limits of 0.2 $\mu\text{g/L}$ and 0.1 $\mu\text{g/L}$, respectively. The NH_4^+ content was detected by an automatic continuous flow analyzer (Auto Analyzer3, Bronrupee, Hamburg, Germany) with a detection limit of 0.02 mg/L. The concentration of REE was determined by high resolution inductively coupled plasma mass spectrometry (HR-ICP-MS, ThermoFisher, Waltham, MA, USA) [23], and its detection limit was 0.5 ng/L. TVOC was measured by the PhoCheck Tiger portable VOC gas detector (PhoCheck Tiger, London, UK), and Rn was

analyzed by the RAD7 radon gas detector (DurrIDGE, Waltham, MA, USA). The analytical error of main and trace chemical components of water samples was better than 5%.

3. Results

3.1. CO₂, TVOC, and Rn Anomalies of the Boiling-Wells

The analysis of gas components (Table 1) documents that the gas in the studied water samples of the six Boiling-Wells, the boiling lake, and the common shallow well is dominated by CO₂, with subordinate Rn and TVOC.

Table 1. Average contents of different gases in water samples and their boiling degree and turbidity state ¹.

Site Name	Free CO ₂ (mg/L)	pH	Rn (pCi/L)	TVOC (µg/L)	Boiling Degree	Turbid State
BW1	439	6.25	962	0.013	Strongest	limpid
BW2	476	6.54	694	0.021	Strong	limpid
BW3	464	5.61	709	0.015	weak	limpid
BW4	453	6.00	857	0.014	Strong	Turbid
BW5	491	4.52	520	0.017	weakest	Turbid
BW6	447	5.12	843	0.019	moderate	Turbid
BL7	bdl	5.24	bdl	bdl	very weak	limpid
BSG8	bdl	8.88	bdl	bdl	no boiling	limpid

Note: “bdl”: below the detection limit. ¹ The contents of Rn and TVOC were measured on the surface of the wells and the lake. The content of TVOC represents the average value of continuous measurement for 2 h.

The content of free CO₂ in the studied water samples of the Boiling-Wells was extraordinarily high, ranging from 439 to 491 mg/L, with an average of 461.67 mg/L. In contrast, the content of free CO₂ in the groundwater of the common shallow well and the boiling lake was below the detection limit. The pH of Boiling-Wells water decreased with the increase of the free CO₂ content, indicating that the water of Boiling-Wells is carbonated.

Our investigations demonstrate that organic pollution sources are lacking around the Boiling-Wells, precluding an external pollution source of TVOC. TVOC was detected in the Boiling-Wells, with concentrations ranging from 0.013 to 0.021 µg/L, but it was absent in the surrounding air, boiling lake water, and shallow groundwater well water.

The concentration of Rn was relatively high around the Boiling-Wells (Table 1), but it was negligible in the surrounding air, lake water, and shallow groundwater well water. The Rn contents in the Boiling-wells water ranged from 962 pCi/L (Sample BW1) to 520 pCi/L (Sample BW5). BW1 showed the highest intensity, indicating that the Rn increased with rising intensity of the boiling (Table 1). The data suggest that the well represented by Sample BW1 has a better connectivity with deep faults.

3.2. Hydrochemical Anomalies of the Boiling-Wells

The hydrochemical analyses show that the contents of Pb²⁺, Al³⁺, Fe²⁺, Mn²⁺, K⁺, Ca²⁺, HCO₃⁻, total hardness, and TDS (Total Dissolved Solid) in the Boiling-Wells were significantly higher than those in surrounding shallow wells (Table 2). Their average values were 12,145%, 4088%, 3493%, 581%, 393%, 276%, 248%, 199%, and 105% higher than those in the surrounding shallow groundwater. Moreover, the contents of H₂SiO₃, As, Zn²⁺, Mg²⁺, Cl⁻, SO₄²⁻, and F⁻ were slightly higher in the Boiling-Wells than in the shallow wells. The contents of COD_{Mn}, pH, and Na⁺ were slightly lower than in the shallow wells. Their mean values were 20.3%, 16.6% and 31.0% lower than those in the surrounding shallow groundwater. The average content of NO₃⁻ in the Boiling-Wells was 97% lower than that in surrounding shallow wells.

Table 2. Hydrochemical compositions of Boiling-Wells and peripheral wells.

Parameters	Boiling-Wells				Surrounding Wells				$\frac{\text{Mean}_B - \text{Mean}_C}{\text{Mean}_C} \%^1$
	Max	Min	Mean	SD	Max	Min	Mean	SD	
K ⁺ (mg/L)	45.6	15.6	37.8	10.1	58.8	0.4	7.7	14.1	392.6%
Na ⁺ (mg/L)	50.2	33.9	37.5	5.8	108.6	13.9	54.3	21.3	−31.0%
Ca ²⁺ (mg/L)	375.5	203.3	299.1	56.0	119.5	29.6	79.5	19.8	276.1%
Mg ²⁺ (mg/L)	40.9	35.1	36.7	2.0	43.6	8.1	25.9	7.5	42.1%
HCO ₃ [−] (mg/L)	1289.0	618.0	1009.8	214.5	589.7	47.6	290.3	110.7	247.9%
SO ₄ ^{2−} (mg/L)	118.0	66.4	101.1	16.9	170.0	22.0	74.6	33.2	35.5%
Cl [−] (mg/L)	188.0	70.6	92.6	42.8	135.0	20.5	65.7	28.3	41.0%
NO ₃ [−] (mg/L)	5.3	0.1	1.0	1.9	144.0	0.0	29.6	31.4	−96.7%
H ₂ SiO ₃ (mg/L)	54.6	48.7	51.8	2.1	44.1	18.4	26.5	6.4	95.0%
F [−] (mg/L)	0.7	0.5	0.6	0.1	3.0	0.1	0.5	0.5	17.6%
Fe ²⁺ (mg/L)	17.0	3.0	11.2	4.4	3.3	0	0.3	0.6	3493.0%
Mn ²⁺ (mg/L)	5.8	1.2	3.4	1.3	9.1	0	0.5	1.6	580.8%
Al ³⁺ (mg/L)	4.8	0.1	1.4	1.6	0.4	0	0	0.1	4088.3%
Pb ²⁺ (μg/L)	55.0	2.0	19.7	17.9	2.0	0	0.2	0.4	12,145.3%
As (μg/L)	8.5	1.5	5.7	2.7	48.1	0	3.8	8.3	51.1%
Zn ²⁺ (mg/L)	0.1	0	0	0	0.2	0	0	0	46.3%
Total hardness(mg/L)	1102.0	702.0	918.2	129.4	469.1	107.0	307.2	71.6	198.9%
TDS (mg/L)	1386.0	1012.0	1176.7	136.8	836.0	211.0	572.8	145.1	105.4%
COD _{Mn} (mg/L)	1.6	1.0	1.4	0.2	7.2	0.5	1.8	1.5	−20.3%
pH	4.5	6.5	5.7	0.8	8.9	5.8	6.8	0.6	−16.6%

¹ Mean_B represents the average water chemical index of Boiling-Wells samples; Mean_C represents the average water chemical index of peripheral wells samples.

The Gibbs diagram that was based on the chemical data of the groundwater shows the relationship between TDS and the ratios of cations and anions (Figure 3) and is a powerful tool to analyze the chemical origin of groundwater [24–26]. It is widely used to explain the mechanism of atmospheric precipitation, rock weathering (water–rock interaction), evaporation, concentration, and other processes that control the chemistry of groundwater [27]. An increase of evaporation and concentration will increase the amount of Na⁺ and Cl[−] in the water body and will decrease the concentration of Ca²⁺ and HCO₃[−]. However, the Boiling-Wells samples clearly differ from the other shallow wells samples (Figure 3). The deviation of Boiling-Wells in the Gibbs diagram indicates that it has undergone different chemical processes from common shallow water.

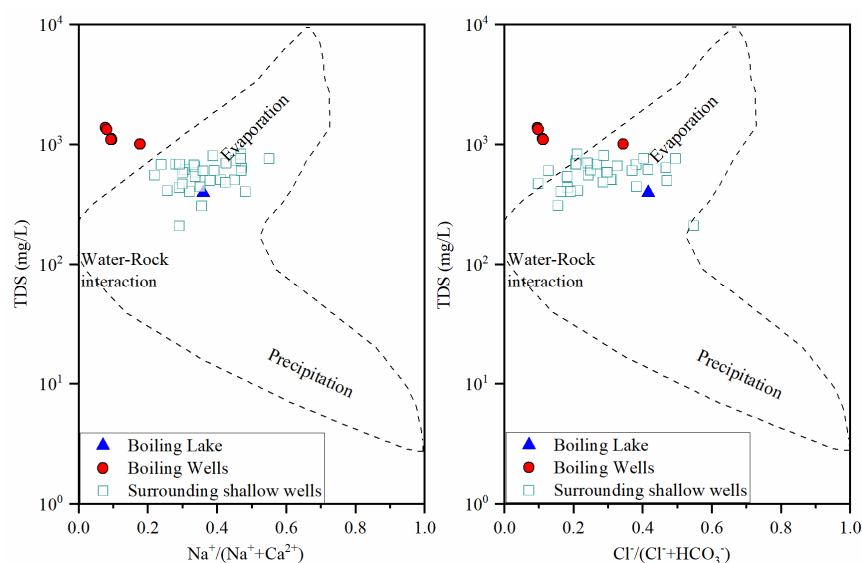


Figure 3. Gibbs figures of the samples in the study area.

3.3. REE Anomalies of the Boiling-Wells

The REE contents of the studied samples are summarized in Table 3. The Σ REE contents in the Boiling-Wells (Sample BW1 to BW6) ranged from 3.5800 to 314.5880 $\mu\text{g/L}$. The Σ REE contents in the lake water (Sample BL7) and shallow well (Sample BSG8) were 44.0220 and 1.5150 $\mu\text{g/L}$, respectively.

Table 3. Concentration of REE($\mu\text{g/L}$) in MBW and peripheral wells.

Parameters	BW1	BW2	BW3	BW4	BW5	BW6	BL7	BSG8
La	58.1750	1.0020	0.7590	8.1990	6.2840	1.1290	8.7590	0.3240
Ce	138.9280	1.6320	1.1300	18.2230	13.6180	2.0410	18.1080	0.4220
Pr	14.3150	0.2300	0.1810	1.9760	1.4900	0.2760	2.1730	0.0810
Nd	52.9760	0.7070	0.5040	7.3130	5.4880	0.9400	7.3760	0.2220
Sm	10.6910	0.1460	0.1110	1.3200	1.0140	0.1900	1.4810	0.0510
Eu	3.6480	0.4340	0.3800	0.9600	0.7640	0.2940	0.9760	0.1260
Gd	10.0240	0.1550	0.1180	1.3310	1.0300	0.2070	1.4640	0.0630
Tb	4.0020	0.0730	0.0600	0.5430	0.4110	0.0900	0.5980	0.0350
Dy	8.6620	0.1170	0.0890	1.0540	0.7010	0.1280	1.1760	0.0420
Ho	1.6020	0.0410	0.0370	0.2210	0.1480	0.0420	0.2340	0.0250
Er	6.3260	0.1070	0.0860	0.8430	0.6050	0.1240	0.8970	0.0420
Tm	0.5380	0.0300	0.0300	0.0930	0.0660	0.0320	0.0920	0.0230
Yb	4.0850	0.0750	0.0650	0.5650	0.3840	0.0870	0.5850	0.0350
Lu	0.6160	0.0320	0.0300	0.1010	0.0750	0.0300	0.1030	0.0240
Σ REE	314.5880	4.7810	3.5800	42.7420	32.0780	5.6100	44.0220	1.5150
$(\text{La}/\text{Yb})_{\text{N}}$ ¹	1.3796	1.2943	1.1312	1.4058	1.5853	1.2571	1.4505	0.8968
δEu ²	1.5472	12.6667	14.5780	3.1799	3.2823	6.5088	2.9102	9.7596

¹ N indicates North American shale calculated values: $(\text{La}/\text{Yb})_{\text{N}} = \text{La}_{\text{N}}/\text{Yb}_{\text{N}}$; ² $\delta\text{Eu} = \text{Eu}_{\text{N}}/\sqrt{\text{Sm}_{\text{N}}*\text{Gd}_{\text{N}}}$.

We collected REE data of shallow groundwater in typical plain basins of China (Jianghan Plain [28], Datong Basin [29], Suzhou Plain [23]) for a comparative analysis. All the data was normalized to North American shale (NASC) [30,31], and the normalized REE distribution patterns are shown in Figure 4. The normalized REE values of the Boiling-Wells ranged from 10^{-4} to 10^{-3} orders of magnitude, and they revealed double-peak patterns with positive Eu and Tb anomalies. The normalized REE values of shallow groundwater for the Jianghan Plain, Datong Basin, and Suzhou Plain in northern Anhui Province were more depleted and ranged from 10^{-7} to 10^{-5} orders of magnitude, and they revealed single-peak patterns with a strong positive Eu anomaly.

In Figure 5, we compare the $(\text{La}/\text{Yb})_{\text{N}}$ and δEu data between the Boiling-Wells with other plain basins of China. The δEu values of the Boiling-Wells water ranged from 1.5472 to 14.5780, with a lower average value of 6.9605 compared with other plains. The $(\text{La}/\text{Yb})_{\text{N}}$ values of the Boiling-Wells ranged from 1.1312 to 1.5853, with an average of 1.3592, showing a depletion of the HREE. However, the average values of $(\text{La}/\text{Yb})_{\text{N}}$ of shallow groundwater in other plain basins of China were significantly lower than that of the Boiling-Wells and lower than 1, indicating that general shallow groundwater is enriched in HREE.

Through the data comparison, the REE patterns, Σ REE, and $(\text{La}/\text{Yb})_{\text{N}}$ were significantly different from those in general shallow groundwater, indicating that its genesis and sources are different from those of general shallow groundwater.

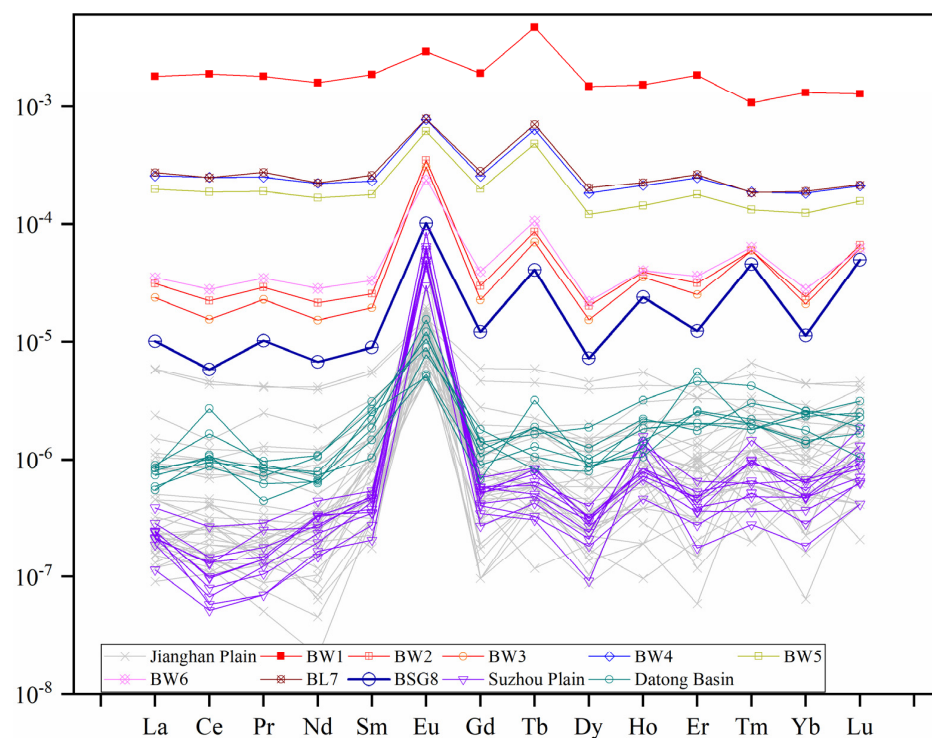


Figure 4. North American shale calculated (NASC) REE patterns in groundwater from the study area and other plains.

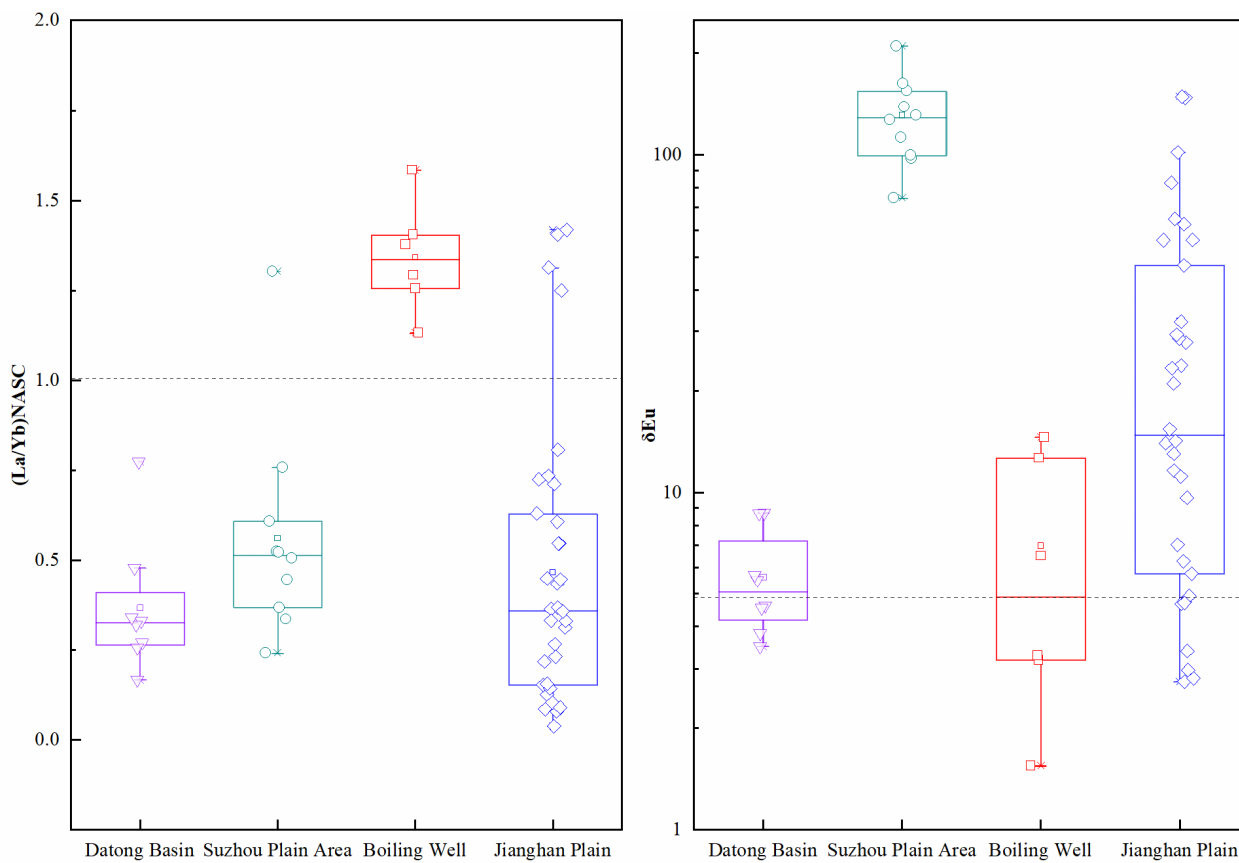


Figure 5. Comparison of groundwater $(La/Yb)_{NASC}$ and δEu between Boiling-Wells and other plain areas.

4. Discussion

4.1. Link between CO₂, Rn, and TVOC Anomalies in Boiling-Wells and the Maodong Fault

Cenozoic basalts are intermittently distributed along the Maodong Fault [16,32]. The basalts contain xenoliths of upper mantle herzolite. A depth of >50 km is constrained for the basaltic melt, indicating that the Maodong Fault may have reached the upper mantle [15–17,33,34]. Previous studies have demonstrated that CO₂ gas reservoirs in eastern China are temporally and spatially related to Cenozoic basalts and probably originated from the upper mantle [35–39]. On a global scale, the distribution of areas that are characterized by the release of mantle-derived CO₂ is often related to seismically active fault zones, indicating that the release of the CO₂-rich mantle fluids is controlled by deep seated faults [37,40,41].

Compared with common well water, the most obvious abnormality in Boiling-wells is the boiling phenomenon caused by the continuous emergence of CO₂. The studied Boiling-Wells of the Maodong Fault Zone and the underlying strata were intruded by dolerites that are related to the basalt emplacement. In addition, bubbles also appear in lakes, ponds, and ditches along the strike of the Maodong Fault. Therefore, we propose that the CO₂ in the Boiling-Wells was sourced from the Cenozoic mantle-derived basaltic melt and associated intrusive rocks and was introduced into the Boiling-Wells along the Maodong Fault.

Previous studies have documented that the gas in the deep mantle degassing zone contains hydrocarbons (a kind of TVOC) [42,43]. Moreover, gas of the Huangqiao CO₂ gas field that occurs 100 km to the northeast of the Maodong Fault contains trace amounts of mantle-derived TVOC [44–46]. Based on data of field tests, TVOC has been documented in the Boiling-Wells, but it was absent in the nearby shallow groundwater wells. Figure 6 shows the positive correlation of the TVOC concentration and the free CO₂ in the Boiling-Wells. Therefore, we propose that the CO₂ in the Boiling-Wells originated from mantle-derived magmas, similar to the Huangqiao Gas Field. This observation further corroborates that both TVOC and CO₂ in the studied Boiling-Wells were sourced from mantle degassing and subsequently migrated upward along the Maodong Fault.

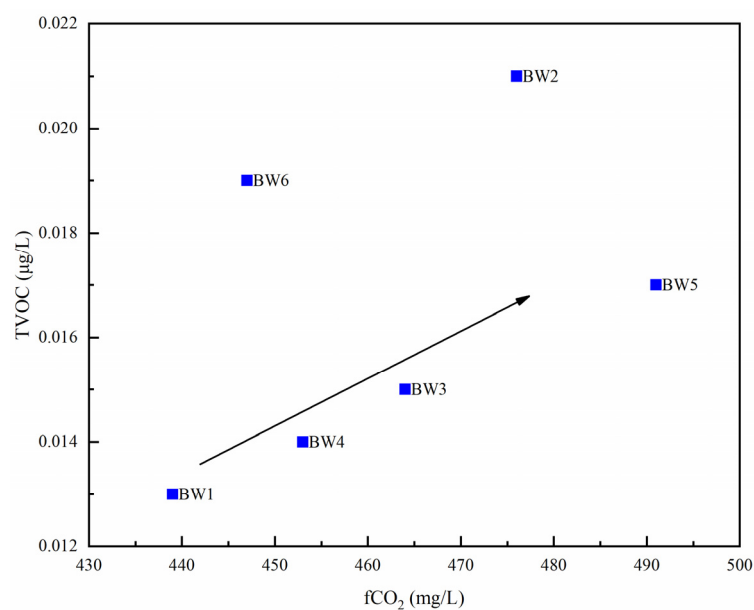


Figure 6. Relationship between TVOC and free CO₂ in the Boiling-Wells.

Radon commonly associates fracture zones and migrates to the surface along faults and associated fracture zones [1]. The content of Rn in the atmosphere is generally much lower than 3 pCi/L [47] in areas without a fault. Previous studies documented a striking correlation between the distribution of high Rn contents in the atmosphere and the distri-

bution of active faults and earthquakes in many cases [48–50]. With the accumulation of stress and strain along active faults, an exceptionally high concentration of Rn may occur. Therefore, Rn is often used to trace the location and intensity of faults [48,51–54].

The striking Rn enrichment in the Boiling-Wells (Table 1) further confirms that the formation of the Boiling-Wells was closely related to the Maodong Fault. However, as the half-life of Rn is only 3.85 days, and the migration rate is low, the migration distance of Rn is very limited. Therefore, a corresponding gas is usually required as a carrier of Rn to migrate [55]. Previous studies have documented that CO₂ can effectively act as a carrier gas for Rn [56,57], indicating the potential of Rn to migrate to the surface along faults. Therefore, the coupled CO₂ and Rn enrichment in the studied Boiling-Wells can be explained by the following model: Mantle-sourced CO₂ carried Rn to the surface along the Maodong Fault, migrated to the Boiling-Wells, and was finally released to the atmosphere.

Based on our new geochemical data, we propose that (1) CO₂ and TVOC in the studied Boiling-Wells were both derived from mantle-derived Cenozoic magmatism and that the origin of Rn is closely related to the tectonic activities in the Maodong Fault; (2) CO₂, TVOC, and Rn all migrated to the Boiling-Wells along the Maodong Fault. Therefore, the Boiling-Wells are excellent “windows” to detect geogas anomalies caused by the Maodong Fault.

4.2. Geochemical Significance of REE Anomalies in Boiling-Wells

REE usually show a consistent geochemical behavior in water and are widely used to trace hydrogeological processes [58–60]. REE concentrations and fractionation patterns of groundwater are usually suitable to constrain the evolution of the aquatic system during the flow in the aquifer rocks [58–60]. During the supergene evolution, the LREE (Light REE) mainly existed in the form of LnCO₃⁺ in the groundwater, whereas the HREE mainly existed in the form of Ln(CO₃)₂[−]. The LREE are more easily adsorbed by aqueous media, whereas the HREE (Heavy REE) tend to remain in the water. Therefore, supergene processes often cause an enrichment of the HREE in the groundwater [60]. The normalized REE data in the studied Boiling-Wells clearly differ from that of common groundwater. Mainly, the positive Eu and Tb anomalies of the REE patterns and the marked LREE enrichment (Table 3, Figures 4 and 5) indicate that the source of the REE in the Boiling-Wells is different from common shallow groundwater. Furthermore, supergene processes can be excluded for the REE enrichment in the Boiling-Wells based on our data.

HCO₃[−] can form a stable complex with the REE, and therefore, high concentrations of HCO₃[−] may cause an increase of the REE concentration in water [29,58,61]. However, the contents of LREE and HREE both decreased with an increasing HCO₃[−] concentration in the Boiling-Wells samples. While the decrease of LREE content was steep, the decrease of HREE content was comparably low (Figure 7). The data further prove that the main sources of the REE in the Boiling-Wells were different from those in common groundwater, that were mainly derived from supergene processes, and confirm our model that the REE in the Boiling-Wells were mainly sourced from mantle-derived CO₂ fluids related to the Cenozoic magmatism. With the emission of CO₂, REE were induced into the Boiling-Wells on the Earth’s surface. However, due to supergene processes, the concentration of REE in the water was reduced, finally resembling that of common shallow groundwater. Moreover, the original enrichment of the LREE gradually disappeared, the REE distribution curve was flattened, and the HREE became slightly enriched.

Loess of the Xiashu Formation is the dominant lithology of the water-bearing medium in the Boiling-Wells. Underlying rocks comprise Cretaceous siltstones and mudstones that are locally intruded by Cenozoic basalts (dolerites). Previous studies have documented the presence of CO₂-rich fluid inclusions in the Cenozoic basalts and dolerites of the study area and in other magmatic rocks from eastern China [62]. CO₂-rich fluids from mantle-derived magmas may transport REE and may cause an enrichment of the LREE through fractionation processes [63–65].

To further refine the source of the REE in the Boiling-Wells, their REE contents were compared to those of Cenozoic basalts [66,67] and loess of the Xiashu Formation [68].

After normalization to the NASC, the Cenozoic basalts displayed enrichment of the LREE, with a moderate positive Eu anomaly and slightly negative Ce anomaly (Figure 8). The LREE patterns of the Boiling-Wells samples generally resembled those of the Cenozoic basalts but were clearly distinct from those of the loess of the Xiashu Formation. In contrast, the HREE characteristics of the Boiling-Wells resembled those of the loess but were different from those of the basalts. The data indicate that the REE characteristics of the Boiling-Wells were related to the input of mantle-derived CO₂ fluid but also to sorption and desorption processes related to the hosting loess of the Xiashu Formation during the supergene evolution.

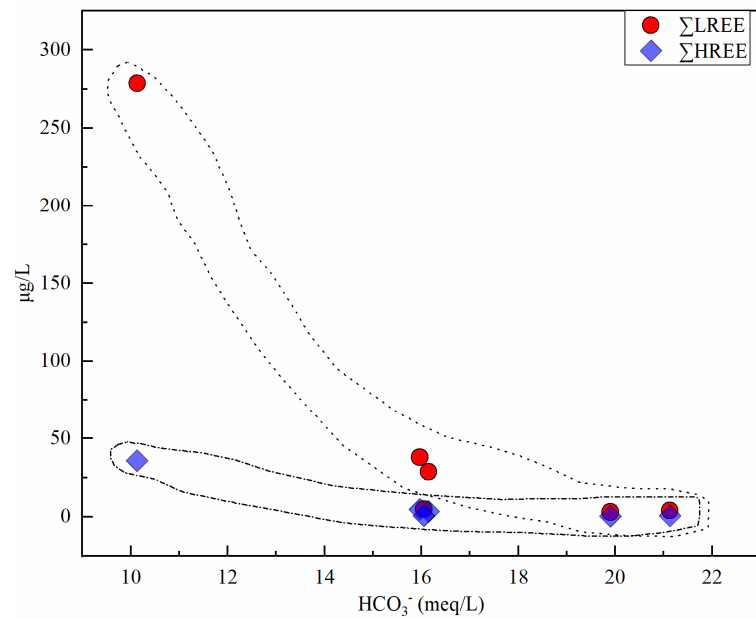


Figure 7. Relationship between Σ LREE, Σ HREE, and HCO_3^- in Boiling-Wells water.

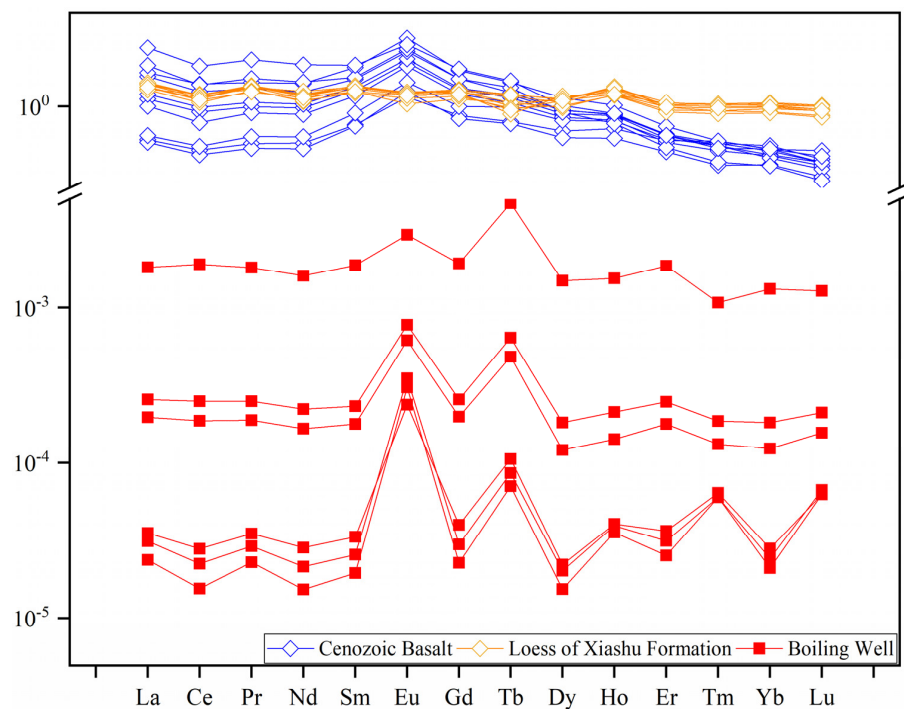


Figure 8. NASC-normalized REE patterns of Boiling-Wells, Cenozoic basalt, and Loess of the Xiashu Formation.

The REE anomalies in the Boiling-Wells document a minor impact of supergene processes. The REE predominantly originated from REE-rich CO₂ fluids that were related to mantle-derived Cenozoic magmas.

4.3. Relationship between Water Chemistry Anomaly of the Boiling-Wells and the Activity of the Maodong Fault

The composition of groundwater affected by tectonic activity in fault zones or by earthquakes will be exceptional, and the injection of CO₂ is proposed as a main mechanism for the generation of the abnormalities [1–6].

According to our investigation, the aquifer medium and discharge path of the Boiling-Wells are the same as those of the surrounding shallow wells. However, water in the Boiling-Wells had an exceptional high concentration of Ca²⁺ and HCO₃[−] (Table 2). Choi et al. [69] studied carbonated groundwater in Korea and documented the input of mantle-derived CO₂ into the carbonated groundwater. The carbonation process can increase the contents of specific ions in the groundwater, particularly of HCO₃[−], Ca²⁺, and TDS. Koh et al. [70] reported the input of magmatic CO₂ into the basalt aquifer of Jeju Island (South Korea), which caused an increase of dissolved inorganic carbon (DIC, including free CO₂, H₂CO₃, HCO₃[−], and CO₃^{2−}) in the water, attaining up to 10 mM/L. High anomalies of HCO₃[−] and Ca²⁺ in the studied Boiling-Wells are consistent with the findings of Choi et al. [69] who proposed that the hydrochemical anomalies in the Boiling-Wells could be related to the input of CO₂-rich fluids.

Enrichment of Pb²⁺ and Al³⁺ in the studied Boiling-Wells (Table 2), which are rather immobile during epigenetic geochemical processes, indicates that these components originated from different sources. An abnormal increase of B was observed in the Deacontr Spring (located in the central Apennines, Italy) prior to the Collelongo earthquake (M4.1) in 2019. The B enrichment was attributed to the desorption of B from aquifer media, which was caused by deep CO₂ degassing [71]. Therefore, we provisionally propose that migration of externally derived (deep) CO₂ could trigger the desorption of additional Pb²⁺ and Al³⁺ as well as other elements in the studied Boiling-Wells. The variations of the Pb²⁺ and Al³⁺ contents are very consistent and generally correlate with an increase of the Rn content (Figure 9). Therefore, we suggest that the enrichment of Pb²⁺ and Al³⁺ in the Boiling-Wells is closely related to the activity of the Maodong Fault.

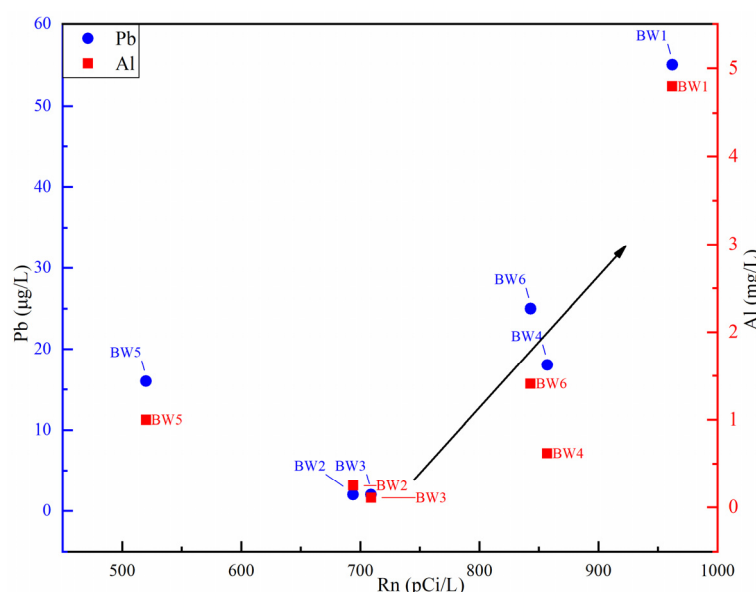


Figure 9. Relationship between Pb, Al, and Rn in Boiling-Wells water.

5. Conclusions

The Maodong Fault (eastern China) was mainly active during the Late Pleistocene. However, in the past century, earthquakes of magnitude 4.5 or higher have occurred along the fault, indicating that the fault is still active. Therefore, it is necessary to strengthen the monitoring of the tectonic activities of the fault [15,72–74]. Water of the long-lasting Boiling-Wells in Jiuli Village, Danyang City, Jiangsu Province (China) was investigated to study the potential of the wells for tracing seismic activity along fault zones. The hydrochemical and gas components, such as CO₂, Rn, TVOC, and REE, of the water in the Boiling-Wells and in surrounding shallow wells were analyzed. Water in the six Boiling-Wells had high concentrations of CO₂, Rn, TVOC, Ca²⁺, HCO₃[−], Pb²⁺, Al³⁺, and ΣREE, as well as REE distribution patterns that significantly differ from common shallow groundwater. Through a comparison of our field investigations and our new analytical data with published data for similar areas, we obtained the following conclusions:

- (1) CO₂ and TVOC in the Boiling-Wells originated from Cenozoic magmatism and associated intrusive rocks. High concentrations of Rn are closely linked to tectonic activities of the Maodong Fault. CO₂, TVOC, and Rn are all transported to the Boiling-Wells along the Maodong Fault, with CO₂ acting as a carrier gas for Rn.
- (2) REE in the Boiling-Wells was mainly sourced from CO₂ fluids that originated from deep-seated Cenozoic magmas and intrusive rocks. The concentrations of the REE and their distribution patterns were controlled by the input of CO₂ fluids and by epigenetic processes.
- (3) The abnormally high contents of Ca²⁺, HCO₃[−], Pb²⁺, and Al³⁺ in the Boiling-Wells are attributed to the migration of externally-derived (deep) CO₂ fluids through the Maodong Fault.
- (4) The anomalies of the gaseous (Rn, CO₂, and TVOC) and hydrochemical components (Ca²⁺, HCO₃[−], Pb²⁺, Al³⁺, ΣREE, and REE patterns) in the Boiling-Wells are closely related to the tectonic activity of Maodong Fault. Therefore, the long-lasting Boiling-Wells provide an excellent geochemical window into the evolution of the Maodong Fault.

Although the anomalies of CO₂, Rn, TVOC, Ca²⁺, HCO₃[−], Pb²⁺, Al³⁺, and ΣREE, as well as the REE distribution patterns in the studied boiling wells, are closely related to the activity of Maodong Fault, the impact of time on the variation of the chemical compositions and the related activities of Maodong Fault (especially seismic activity) remains uncertain, so far. Therefore, we will conduct monthly frequency geochemical monitoring of the variation of suitable geochemical tracers that will characterize the tectonic activities of the Maodong Fault, and we will correlate the monitoring data with the overall geostress field in a future project.

Author Contributions: This fieldwork was conducted by L.L., Y.J. (Yuehua Jang), X.Z., Y.L., Q.Z., J.S., J.J., G.Y. and Y.J. (Yang Jin); The manuscript, data analysis, and drawing of this paper were completed by L.L. and Y.J. (Yuehua Jang). All authors have read and agreed to the published version of the manuscript.

Funding: This research was financially supported the China Geological Survey Project ‘Comprehensive Geological Environment Survey Project of the Yangtze River Economic Belt (No. 0531)’ and ‘Comprehensive Evaluation of Geological Resources and Environment of the Yangtze River Economic Belt (DD20190260)’.

Data Availability Statement: The data supporting this article are listed in the tables.

Acknowledgments: Field work was strongly supported by Hongying Liu, Xiaojun Chang, Huaixue Xing, and Fujin Tian from the Nanjing Center, China Geological Survey. The reviewers have played an important role in further improving the quality of this paper by putting forward valuable and constructive suggestions. The authors would like to express their gratitude to EditSprings (<https://www.editsprings.cn/>, accessed on 8 January 2022) for the expert linguistic services provided.

Conflicts of Interest: The authors declare no conflict of interest.

References

1. Walia, V.; Yang, T.F.; Lin, S.-J.; Kumar, A.; Fu, C.-C.; Chiu, J.-M.; Chang, H.-H.; Wen, K.-L.; Chen, C.-H. Temporal variation of soil gas compositions for earthquake surveillance in Taiwan. *Radiat. Meas.* **2013**, *50*, 154–159. [[CrossRef](#)]
2. Tedesco, D.; Scarsi, P. Chemical (He, H₂, CH₄, Ne, Ar, N₂) and isotopic (He, Ne, Ar, C) variations at the solfatar crater (southern Italy): Mixing of different sources in relation to seismic activity. *Earth Planet. Sci. Lett.* **1999**, *171*, 465–480. [[CrossRef](#)]
3. Tsunogai, U.; Wakita, H. Precursory chemical changes in ground water: Kobe earthquake, Japan. *Science* **1995**, *269*, 61–63. [[CrossRef](#)] [[PubMed](#)]
4. Zhou, Z.; Zhong, J.; Zhao, J.; Yan, R.; Tian, L.; Fu, H. Two Mechanisms of Earthquake-Induced Hydrochemical Variations in an Observation Well. *Water* **2021**, *13*, 2385. [[CrossRef](#)]
5. Ma, Y.; Wang, G.; Yan, R.; Wang, B.; Yu, H.; Yu, C.; Yue, C.; Wang, Y. Relationship between Earthquake-Induced Hydrologic Changes and Faults. *Water* **2021**, *13*, 2795. [[CrossRef](#)]
6. Barbieri, M.; Franchini, S.; Barberio, M.D.; Billi, A.; Boschetti, T.; Giansante, L.; Gori, F.; Jonsson, S.; Petitta, M.; Skelton, A.; et al. Changes in groundwater trace element concentrations before seismic and volcanic activities in Iceland during 2010–2018. *Sci. Total Environ.* **2021**, *793*, 148635. [[CrossRef](#)]
7. Sun, X.; Wang, G.; Shao, Z.; Si, X. Geochemical characteristics of emergent gas and groundwater in Haiyuan fault zone. *Earth Sci. Front.* **2016**, *23*, 140–150. (In Chinese) [[CrossRef](#)]
8. Li, Y.; Du, J.; Wang, F.; Zhou, X.; Pan, X.; Wei, R. Geochemical characteristics of soil gas in the Yanhuai basin, northern China. *Earthq. Sci.* **2009**, *22*, 93–100. [[CrossRef](#)]
9. Perrier, F.; Richon, P.; Byrdina, S.; France-Lanord, C.; Rajaure, S.; Koirala, B.P.; Shrestha, P.L.; Gautam, U.P.; Tiwari, D.R.; Revil, A.; et al. A direct evidence for high carbon dioxide and radon-222 discharge in Central Nepal. *Earth Planet. Sci. Lett.* **2009**, *278*, 198–207. [[CrossRef](#)]
10. Annunziatellis, A.; Beaubien, S.; Bigi, S.; Ciotoli, G.; Coltella, M.; Lombardi, S. Gas migration along fault systems and through the vadose zone in the Lateral caldera (central Italy): Implications for CO₂ geological storage. *Int. J. Greenh. Gas Control* **2008**, *2*, 353–372. [[CrossRef](#)]
11. Zhang, M.; Guo, Z.; Xu, S.; Barry, P.H.; Sano, Y.; Zhang, L.; Halldorsson, S.A.; Chen, A.T.; Cheng, Z.; Liu, C.Q.; et al. Linking deeply-sourced volatile emissions to plateau growth dynamics in southeastern Tibetan Plateau. *Nat. Commun.* **2021**, *12*, 4157. [[CrossRef](#)] [[PubMed](#)]
12. Seminsky, K.Z.; Demberel, S. The first estimations of soil-radon activity near faults in Central Mongolia. *Radiat. Meas.* **2013**, *49*, 19–34. [[CrossRef](#)]
13. Li, G. The preliminary study on hydrogeochemistry precursor anomaly and short-imminent term forecast criterion for earthquake (Ms>5.0) in ningxia and vicinity. *Inland Earthq.* **1992**, *6*, 106–114. (In Chinese)
14. Meng, G.; He, K.; Ban, T.; Jiao, D. Study on activity and segmentation of active fault using measurements of radon and mercury gases. *Earthq. Res. China* **1997**, *13*, 45–50. (In Chinese)
15. He, Z. Investigation and Study on the Late Quaternary Activity of Maodong Fault Zone in the Central Part of Southern Jiangsu. Master's Thesis, Chengdu University of Technology, Chengdu, China, 2020. (In Chinese).
16. Zong, K.; Zong, W.; Kang, C.; Bai, S. Research on the major active faults in Zhenjiang, Jiangsu and their late Quaternary activities. *J. Geomech.* **2016**, *22*, 439–453. (In Chinese)
17. Hu, L.; Xu, X. An analysis of geological factors for the occurrence and gestation in Liyang earthquake. *Jiangsu Geol.* **2001**, *25*, 11–16. (In Chinese)
18. Gao, X.; Hu, L.; Xu, X.; Sun, S. A dynamic model of eastern Maoshan's fault movement relating to Liyang earthquake. *J. Seismol. Res.* **1993**, *16*, 401–409. (In Chinese)
19. Gao, Z.; Hu, L.; Sun, S.; Zheng, Q. On the relations between deep-seated crustal structures and genesis of Liyang earthquakes in Maoshan area—a new ideas. *J. Seismol.* **1989**, *2*, 37–47. (In Chinese)
20. Jiang, Y.; Zhou, Q.; Li, Y.; Su, J.; Zhang, T.; Jia, J.; Ge, W.; Yang, H.; Liu, L.; Yang, G.; et al. Geological origin and formation mechanism of the millennium “boiling well” in Danyang, Jiangsu Province. *Acta Geol. Sin.* **2019**, *93*, 1778–1791. (In Chinese) [[CrossRef](#)]
21. Hydrogeological Team of Jiangsu Geological Bureau. *Regional Hydrogeological Survey Report of the People's Republic of China (Changzhou)*; Hydrogeological Team of Jiangsu Geological Bureau: Nanjing, China, 1979; p. 5.
22. Li, Q.; Zhu, Q.; Hu, L. Review on geological and seismic studies in Maoshan, Jiangsu province. *J. Seismol.* **1983**, *2*, 63–71. (In Chinese)
23. Min, N.; Cui, H.; He, S. Determination of trace rare earth elements in water by HR-ICP-MS method. *J. Suzhou Univ.* **2017**, *32*, 117–119, 124. (In Chinese) [[CrossRef](#)]
24. Wang, Y.; Wang, L.; Xu, C.; Yang, Z.; Ji, J.; Xia, X.; An, Z.; Yuan, J. Hydro-geochemistry and genesis of major ions in the Yangtze River, China. *Geol. Bull. China* **2010**, *29*, 446–456. (In Chinese)
25. Gibbs, R.J. Mechanisms controlling world water chemistry. *Science* **1970**, *170*, 1088–1090. [[CrossRef](#)] [[PubMed](#)]
26. Feth, J.H.; Gibbs, R.J. Mechanisms controlling world water chemistry: Evaporation-crystallization process. *Science* **1971**, *172*, 870–872. [[CrossRef](#)] [[PubMed](#)]
27. Raju, N.J.; Shukla, U.K.; Ram, P. Hydrogeochemistry for the assessment of groundwater quality in Varanasi: A fast-urbanizing center in Uttar Pradesh, India. *Environ. Monit. Assess.* **2011**, *173*, 279–300. [[CrossRef](#)] [[PubMed](#)]

28. Zheng, T.; Deng, Y.; Lu, Z.; Gan, Y. Geochemistry and implications of rare earth elements in arsenic-affected shallow aquifer from Jiangnan plain, central China. *Earth Sci.* **2017**, *42*, 693–706. (In Chinese) [[CrossRef](#)]
29. Xie, X.; Wang, Y.; Li, J.; Su, C.; Wu, Y.; Yu, Q.; Li, M. Characteristics and Implications of Rare Earth Elements in High Arsenic Groundwater from the Datong Basin. *Earth Sci.* **2012**, *37*, 381–390. (In Chinese) [[CrossRef](#)]
30. Haskin, M.A.; Haskin, L.A. Rare Earths in European Shales: A Redetermination. *Science* **1966**, *154*, 507–509. [[CrossRef](#)]
31. Haskin, M.A.; Haskin, L.A.; Frey, F.A. *Wildeman, Relative and Absolute Terrestrial Abundances of the Rare Earths*; Elsevier Ltd.: Amsterdam, The Netherlands, 1968; pp. 889–912. [[CrossRef](#)]
32. Jiang, G. A exploration of recent tectonic stress field from remote sensing geology in Maoshan and adjacent region. *J. Seismol.* **1989**, *2*, 65–68. (In Chinese)
33. Guo, Y.; Li, Q. The study history on seismo-geology and its relation to the occurrence of earthquakes in Maoshan district. *J. Seismol.* **1989**, *10*, 1–5. (In Chinese)
34. Chen, D.; Peng, Z. K-Ar ages and Pb, Sr isotopic characteristics of some Cenozoic volcanic rocks from Anhui and Jiangsu provinces, China. *Acta Petrol. Sin.* **1988**, *4*, 3–12. (In Chinese)
35. Dai, C.; Song, Y.; Sun, Y. Genetic Characteristics and Distribution of Carbon Dioxide Gas Reservoirs in Eastern China. *Sci. China Ser. B* **1995**, *25*, 764–771. (In Chinese) [[CrossRef](#)]
36. He, J.; Xia, B.; Liu, B.; Zhang, S. Origin, migration and accumulation of CO₂ in east China and offshore shelf basins. *Petrol. Explor. Dev.* **2005**, *32*, 42–49. (In Chinese)
37. Lin, S. Fault and Magmatic Activity as Control of Mantle Source CO₂ Gas Accumulation: A Case Study of Jiyang Depression. *Earth Sci.* **2005**, *14*, 3473–3479. (In Chinese)
38. Wang, J.; Liu, W.; Qin, J.; Zhang, J. Mantle-derived gas reservoir and its forming rules in eastern China. *Nat. Gas. Geosci.* **2007**, *18*, 19–26. (In Chinese)
39. Wang, J.; Liu, W.; Qin, J.; Zhang, J.; Shen, B. Reservoir forming mechanism and origin characteristics in Huangqiao carbon dioxide gas field, north Jiangsu Basin. *Nat. Gas. Geosci.* **2008**, *19*, 826–833. (In Chinese)
40. Zhang, J.; Hu, H. Summarization on the researches of the releasing process of the mantle-originated CO₂ through deep faults. *Carsol. Sin.* **1999**, *18*, 95–102. (In Chinese)
41. Tao, M.; Xu, Y.; Shi, B.; Jiang, Z.; Shen, P.; Li, X.; Sun, M. The characteristics of mantle degassing and deep geological structure in different types of fault zones in China. *Sci. China Ser. D* **2005**, *35*, 441–451. [[CrossRef](#)]
42. Luo, Q. Concept, principle, model and significance of the fault controlling hydrocarbon theory. *Petrol. Explor. Dev.* **2010**, *37*, 316–324. (In Chinese)
43. Guo, J. Study on the theory and application of abiogenic natural gas. *Adv. Earth Sci.* **1966**, *11*, 224. (In Chinese)
44. Li, X.; Dai, J. Geochemical characteristics and genetic analysis of CO₂ fields (pools) in east China. *Exp. Pet. Geol.* **1997**, *19*, 215–221. (In Chinese)
45. Dai, J.; Dai, C.; Song, Y.; Hong, F. CO₂ gas reservoirs of inorganic origin and their characteristics in eastern China. *China Offshore Oil Gas (Geol.)* **1994**, *8*, 215–222. (In Chinese)
46. Liao, F.; Wu, X.; Huang, S. Geochemical characteristics of CO₂ gases in eastern China and the distribution patterns of their accumulations. *Acta Petrol. Sin.* **2012**, *28*, 939–948. (In Chinese)
47. Florea, N.; Dului, O.G. Eighteen years of continuous observation of Radon and Thoron progenies atmospheric activity. *J. Environ. Radioact.* **2012**, *104*, 14–23. [[CrossRef](#)] [[PubMed](#)]
48. Han, X.; Li, Y.; Du, J.; Zhou, X.; Xie, C.; Zhang, W. Rn and CO₂ geochemistry of soil gas across the active fault zones in the capital area of China. *Nat. Hazard. Earth Syst. Sci.* **2014**, *14*, 2803–2815. [[CrossRef](#)]
49. Li, Y.; Du, J.; Wang, X.; Zhou, X.; Xie, C.; Cui, Y. Spatial variations of soil gas geochemistry in the Tangshan area of northern China. *Terr. Atmos. Ocean. Sci.* **2013**, *24*, 323–332. [[CrossRef](#)]
50. Woodruff, L.G.; Cannon, W.F.; Eberl, D.D.; Smith, D.B.; Kilburn, J.E.; Horton, J.D.; Garrett, R.G.; Klassen, R.A. Continental-scale patterns in soil geochemistry and mineralogy: Results from two transects across the United States and Canada. *Appl. Geochem.* **2009**, *24*, 1369–1381. [[CrossRef](#)]
51. Singh, S.; Kumar, A.; Bajwa, B.S.; Mahajan, S.; Kumar, V.; Dhar, S. Radon monitoring in soil gas and ground water for earthquake prediction studies in north west Himalayas, India. *TAO Terr. Atmos. Ocean. Sci.* **2010**, *21*, 685–695. [[CrossRef](#)]
52. Kobeissi, M.A.; Gomez, F.; Tabet, C. Measurement of anomalous radon gas emanation across the Yammouneh Fault in southern Lebanon; a possible approach to earthquake prediction. *Int. J. Disaster. Risk Sci.* **2015**, *6*, 250–266. [[CrossRef](#)]
53. Lombardi, S.; Oltattorni, N.V. Rn, He and CO₂ soil gas geochemistry for the study of active and inactive faults. *Appl. Geochem.* **2010**, *25*, 1206–1220. [[CrossRef](#)]
54. Yang, J.; Li, Y.; Chen, Z.; Sun, F.; Zhao, J.; Li, J.; Wang, J. Geochemical characteristics of soil gas in the south-west and north-east segments of the Tangshan fault zone, Northern China. *Earthquake* **2019**, *39*, 61–70. [[CrossRef](#)]
55. Toutain, J.-P.; Baubron, J.-C. Gas geochemistry and seismotectonics: A review. *Tectonophysics* **1999**, *304*, 1–27. [[CrossRef](#)]
56. Etiope, G.; Martinelli, G. Migration of carrier and trace gases in the geosphere; an overview. *Phys. Earth Planet. Inter.* **2002**, *129*, 185–204. [[CrossRef](#)]
57. Yang, T.F.; Chou, C.Y.; Chen, C.-H.; Chyi, L.L.; Jiang, J.H. Exhalation of radon and its carrier gases in SW Taiwan. *Radiat. Meas.* **2003**, *36*, 425–429. [[CrossRef](#)]

58. Zhou, X.; Liu, L.; Ye, Y. Contents and distribution pattern of rare earth elements in phreatic water from Nantong area along the Yangtze river and their hydrochemical indication Significance. *Geol. Sci. Technol. Inf.* **2018**, *37*, 210–218. [[CrossRef](#)]
59. Dia, A.; Gruau, G.; Olivie-Lauquet, G.; Riou, C.; Molenat, J.; Curmi, P. The distribution of rare earth elements in groundwaters; assessing the role of source-rock composition, redox changes and colloidal particles. *Geochim. Cosmochim. Acta* **2000**, *64*, 4131–4151. [[CrossRef](#)]
60. Liu, H.; Guo, H.; Xing, L.; Zhan, Y.; Li, F.; Shao, J.; Niu, H.; Liang, X.; Li, C. Geochemical behaviors of rare earth elements in groundwater along a flow path in the North China Plain. *J. Asian Earth Sci.* **2016**, *117*, 33–51. [[CrossRef](#)]
61. Guo, H.; Zhang, B.; Li, Y.; Wei, L.; Zhang, Y. Concentrations and patterns of rare earth elements in high arsenic groundwaters from the Hetao Plain, Inner Mongolia. *Earth Sci. Front.* **2010**, *17*, 59–66. (In Chinese)
62. Fan, Q.; Liu, R.; Yang, R. LREE-Rich CO₂ fluid inclusions in mantle minerals in eastern China and their geological significance. *Acta Petrol. Sin.* **1993**, *9*, 411–417. (In Chinese)
63. Schrauder, M.; Koeberl, C.; Navon, O. Trace element analyses of fluid-bearing diamonds from Jwaneng, Botswana. *Geochim. Cosmochim. Acta* **1996**, *60*, 4711–4724. [[CrossRef](#)]
64. Schrauder, M.; Navon, O. Hydrous and carbonatitic mantle fluids in fibrous diamonds from Jwaneng, Botswana. *Geochim. Cosmochim. Acta* **1994**, *58*, 761–771. [[CrossRef](#)]
65. Liu, C.; Huang, Z.; Li, H.; Su, G. The geofluid in the mantle and its role in ore-forming processes. *Earth Sci. Front.* **2001**, *8*, 231–244. (In Chinese)
66. Li, Y.; Ma, C.; Robinson, P.T. Petrology and geochemistry of Cenozoic intra-plate basalts in east-central China: Constraints on recycling of an oceanic slab in the source region. *Lithos* **2016**, *262*, 27–43. [[CrossRef](#)]
67. Wang, Y. Geochemical Study of Cenozoic Continental Basalts in Northern Jiangsu-Hefei, Eastern China. Ph.D. Thesis, University of Science and Technology of China, Hefei, China, 2011. (In Chinese).
68. Qi, L.; Qiao, Y.; Wang, Y.; Peng, S.; Yang, S.; Bai, W. Geochemical characteristics of the Xiashu loess-palaeosol sequence in Nanjing and their implications for provenance. *Quat. Sci.* **2020**, *40*, 190–202. [[CrossRef](#)]
69. Choi, H.; Woo, N.C. Natural analogue monitoring to estimate the hydrochemical change of groundwater by the carbonating process from the introduction of CO₂. *J. Hydrol.* **2018**, *562*, 318–334. [[CrossRef](#)]
70. Koh, D.-C.; Genereux, D.P.; Koh, G.-W.; Ko, K.-S. Relationship of groundwater geochemistry and flow to volcanic stratigraphy in basaltic aquifers affected by magmatic CO₂, Jeju Island, Korea. *Chem. Geol.* **2017**, *467*, 143–158. [[CrossRef](#)]
71. Franchini, S.; Agostini, S.; Barberio, M.D.; Barbieri, M.; Billi, A.; Boschetti, T.; Pennisi, M.; Petitta, M. Hydro Quakes, central Apennines, Italy: Towards a hydrogeochemical monitoring network for seismic precursors and the hydro-seismo-sensitivity of boron. *J. Hydrol.* **2021**, *598*, 125754. [[CrossRef](#)]
72. Wu, Z.; Zhou, C.; Huang, X.; Zhao, G.; Tan, C. Main active faults and seismic activity along the Yangtze River Economic Belt: Based on remote sensing geological survey. *China Geol.* **2020**, *3*, 314–338. [[CrossRef](#)]
73. Jiang, Y.; Lin, L.; Chen, L.; Ni, H.; Ge, W.; Cheng, H.; Zhai, G.; Wang, G.; Ban, Y.; Li, Y.; et al. Research on conditions of resources and environment and major geological problems in the Yangtze River Economic Zone. *Geol. China* **2017**, *44*, 1045–1061. (In Chinese) [[CrossRef](#)]
74. Wang, X.; Li, Y.; Du, J.; Chen, Z.; Zhou, X.; Li, X.; Cui, Y.; Wang, H.; Zhang, Z. Geochemical characteristics of soil gases Rn, Hg and CO₂ and their genesis in the capital area of China. *Acta Seismol. Sin.* **2017**, *39*, 85–101. [[CrossRef](#)]